The jets of SS 433: second order effects

W. Brinkmann[1] **and N. Kawai**[2]

[1] Max-Planck-Institut für extraterrestrische Physik, Giessenbachstrasse, 85740 Garching, Germany
[2] Cosmic Radiation Laboratory, RIKEN, 2-1 Hirosawa, Wako-shi, Saitama 351-01, Japan

Abstract. Previous analyses of the X-ray emission from SS 433 have assumed conically out-flowing jets of hot plasma in ionizational equilibrium conditions to deduce the system's physical parameters from the data. Current X-ray instruments are sensitive enough to detect the effects of second order deviations from these simple assumptions in the measured spectra. We have modeled the two dimensional hydrodynamic outflow of the jets with different initial conditions, and considered non-equilibrium effects and photoionization in the plasma. The deviations from the canonical model are discussed and the influence on the determination of the system's physical parameters are evaluated.

Key words: stars: individual: SS433 – X-rays: general – radiation mechanisms: thermal – hydrodynamics

1. Introduction

The Galactic binary SS 433 emits two oppositely directed jets with velocities of $v_j \sim 0.26c$, which precess under an angle of $\theta = 19.8^o$ with a period of $P_p = 163.99$ days (Margon 1984). The kinetic energy of the jets is enormous and might quite well be in excess of $\sim 10^{40}$ erg s^{-1}. The X-ray emission from the jets is predominantly thermal (Watson et al. 1986) and originates from the innermost regions of the jets. It is strongly modulated with both the precessional phase and the binary motion with period $P_b = 13.77$ days (Yuan et al. 1995).

Even 20 years after its detection many details of the system, its evolutionary origin, the nature of the compact object and the jet acceleration mechanism remain poorly understood. However, two aspects of the systems X-ray jets are unique: the length of the jets is of the same order as the dimensions of the binary systems and thus occultation observations can be used to determine directly the size of the primary star and the orbital separation. And, secondly, for an astrophysical system the physical parameters of the jets are exceedingly well determined, all relevant quantities to about an order of magnitude. This still implies large uncertainties in some critical astrophysical parameters of the system, like the mass outflow rate from the compact object

and the energy deposition rate into the surrounding supernova remnant W50. However, the jets present an ideal laboratory for our understanding of the jet phenomenon itself, for comparisons of numerical jet models with observational facts. Along these lines the first time dependent, 3-dimensional simulations of a precessing, hydrodynamical jet have recently shown new insights into the systems' dynamics (Müller et al. 2000).

Our knowledge of the jet's parameters is mainly based on comparisons of simple hydro-dynamical models with the results from X-ray observations (Brinkmann et al. 1989a; Yuan et al. 1995; Kotani et al. 1996). In these models the jet is treated as a hydro-dynamical, purely radially out-flowing conical flow. The plasma is optically thin and in collisional ionization equilibrium (CIE) and all flow parameters depend only on the radial distance from the jet's origin.

These approximations can be justified for a large range of models and so far the deviations from more exact flow solutions could not be tested observationally due to the limited energy resolution and sensitivities of previous X-ray instruments. However, deep ASCA observations (Kotani et al. 1996) allowed for the first time estimates of the jet parameters by emission line diagnostics, using mainly iron, sulfur, and silicon lines. Although this approach promises a much more accurate determination of the physical parameters of the out-flowing plasma, a detailed knowledge of the spatial variations of the jet's X-ray emission is required. The cumulative uncertainties of the line measurements are presently still rather large but a reliable mapping of the emission characteristics of the jets will be feasible with the current generation X-ray missions Chandra and XMM-Newton.

There are basically three areas in which the currently used simplified models might be inappropriate:

– The hydrodynamic outflow can not be purely radial, confined to a cone with constant lateral plasma conditions.
– Depending on the densities of the jet matter the flow time scales might be too short to achieve collisional equilibrium ionization conditions throughout the jet.
– The plasma ionization has been treated in the collisional coronal approximation; the possible role of photo ionization has not been considered.

While the first approximation applies to all kinds of outflow models the two latter effects are density dependent and thus af-

fect any determination of the jet parameters in a non-linear way. In the following, we will study the influence of these currently used approximations on the emission properties of the jets and thus on the intrinsic uncertainties in the determination of the jet properties.

We will compare the X-ray signatures of jets, for which successively the different approximations made above are relaxed, with those obtained from a 'standard' conical jet model. For the basic model we will take jet parameters, typically used in recent X-ray studies.

2. One dimensional jets

In the standard jet model the properties of the jets are determined by only a few free parameters: the temperature T_0 at the base of the cooling jet and the number density n_0 of the plasma. The flow velocity $v_{jet} = 0.26$ c is fixed and the opening angle of the jet is narrowly confined to be smaller than $\Theta = 5^o$ (Shaham 1981). In our models we will use for the half opening angle a fixed value of $\Theta = 2.5^o$. The general effects of changes in Θ on the emitted X-ray spectrum are discussed by Brinkmann et al. (1988). We further adopt a plasma with cosmic abundances and assume purely thermal emission from a gas in collisional ionization equilibrium (CIE) at the local temperature.

In the 'conventional' approach the temperature T_0 is determined by fitting the shape of the continuum spectrum to the observational data. The Ginga measurements indicated rather high temperatures, in excess of $kT_0 = 30$ keV (Brinkmann et al. 1991), sometimes approaching ~ 40 keV (Yuan et al. 1995). The obtained temperatures obviously depend on both, the binary and the precessional phases of the system, i.e., the actual viewing conditions of the inner parts of the jets. Recent observations with ASCA, employing a temperature determination from the measurement of the iron emission line ratios, yield slightly lower temperatures of $kT_0 \sim 22$ keV, however with large errors (Kotani et al. 1996). Throughout this paper we will use an initial temperature of $kT_0 = 20$ keV for all our models.

The value of the density n_0 can be obtained from the normalization of the model spectrum to the measured flux, assuming a distance to the source of ~ 5 kpc. However, this parameter can not be determined uniquely as the spectral information is insufficient to distinguish between a low density, wide jet and a high density, narrow jet. Observations of the eclipse of the jets by the primary star provide the additional information on the radial emission characteristics of the X-ray jet which narrows down the range of possible density values. However, eclipse observations have been rather rare and usually values around $n_0 = 5 \times 10^{13}$ cm^{-3} give acceptable models for the X-ray emission of the jets.

2.1. The standard model

In the following the term 'standard model' refers to a conical jet with $n_0 = 5 \times 10^{13}$ cm^{-3}, $kT_0 = 20$ keV and opening angle $\Theta = 2.5^o$, with the gas in CIE at the local temperature. For the jet matter we assume the cosmic matter composition of Allen
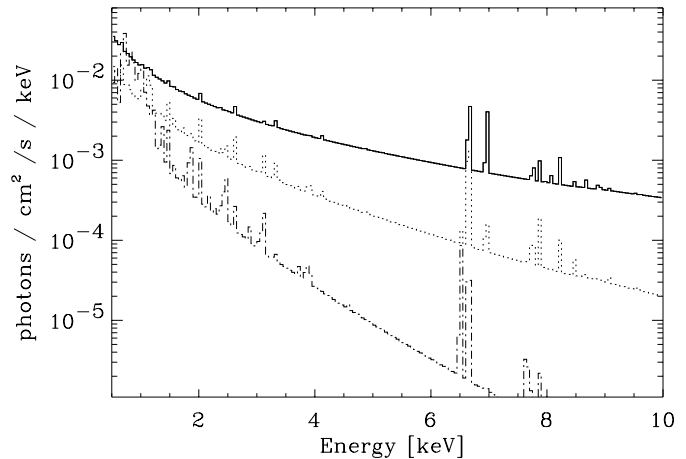

Fig. 1. Photon spectrum emitted from a conical jet. Full line: spectrum emitted from the innermost $\leq 3 \times 10^{11}$ cm from the jet base; dotted line: spectrum emitted at distances 3×10^{11} cm $\leq l \leq 6 \times 10^{11}$ cm; dash-dotted line: spectrum emitted from the outermost $> 6 \times 10^{11}$ cm.

(1973), the ionization and recombination rates are taken from Arnaud & Rothenflug (1985), with corrections for the Fe rates from Arnaud & Raymond (1992). For the calculation of the optically thin X-ray emission we employed the emission model of Mewe et al. (1985).

The photon spectrum emitted from such 'standard' jet is shown in Fig. 1. We did not take into account the Doppler boosting from the out-flowing jets in any of the spectra shown. The full line represents the spectrum, emitted from the innermost 3×10^{11} cm from the jet's base, the dotted line that from distances of $3 \times 10^{11} < l \leq 6 \times 10^{11}$ cm along the jet; the dash-dotted line the emission from the outermost $l > 6 \times 10^{11}$ cm of the jet. It can be seen that the hard X-ray continuum is a very insensitive indicator for the jet length as nearly all the hard emission originates from the inner jet; most of the X-ray flux emitted from the outer jets is found in the soft band. However, in the case of SS 433 the flux below ~ 1 keV is heavily absorbed by cold interstellar gas with column density of $N_H \sim 5.7 \times 10^{21}$ cm^{-2} (Brinkmann et al. 1996) and cannot be detected from Earth. Reversing these arguments implies that observations of the eclipse of the inner parts of the jet by the primary star provides a very sensitive method to determine the geometrical sizes of the system.

The determination of the strengths of various X-ray emission lines by high resolution X-ray detectors provide a new opportunity to map the emission characteristics of the jet. This method is particularly valuable as the use of line ratios of the same element eliminates to a large degree the basic uncertainties about the chemical abundances of the out-flowing gas.

The electron temperature can be diagnosed from the intensity ratio of two collisionally excited lines from different ions of the same element in collisional ionization equilibrium (see, for example, Tanaka 1986). For SS433 this tool has been used for the first time for recent ASCA observations (Kotani et al. 1996) which had, however, limited statistical accuracy. Further, the exact viewing conditions, the temperature distribution along the
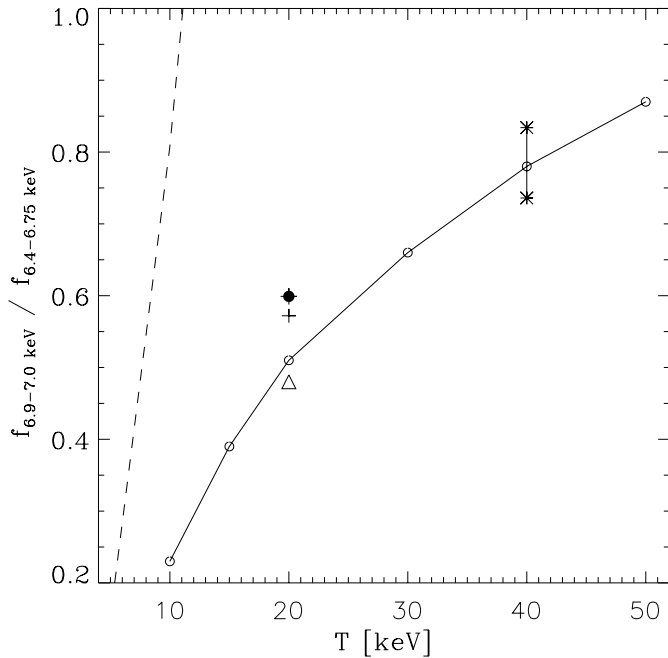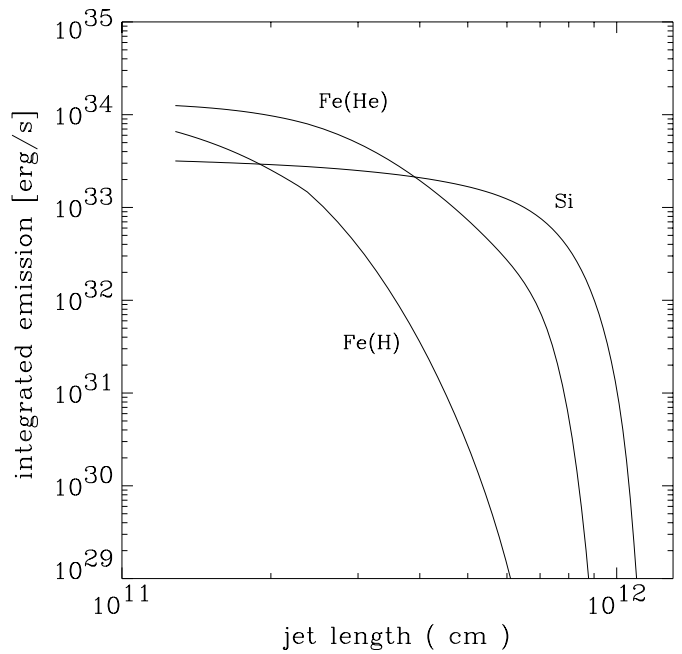
Fig. 2. Iron line flux ratio $f_{6.9-7.0\,\mathrm{keV}}/f_{6.4-6.75\,\mathrm{keV}}$ as function of temperature (in keV). Dashed line: isothermal iron plasma; full line: standard jet with base temperature T_0. Error bar with stars at 40keV: different initial densities of the jet (see text). The other symbols represent models discussed in the text: '+' refers to Gaussian density distribution, filled circle with cross to hydrodynamic outflow, and the triangle to a flow with photoionization.

Fig. 3. Integrated line emission from a conical jet. Given as the function of the jet length is the integrated flux emitted from that length outwards.

out-flowing jets and details of the ionization structure introduce considerable uncertainties and the energy resolution of current CCD detectors is still insufficient to separate the different iron lines in the 6.4–7 keV energy range. We will therefore use the ratio of the lines in the two energy bands 6.4–6.75 keV and 6.9–7.0 keV, which contain mostly FeXXV and FeXXVI emission lines as temperature indicators. We will denote them in the following as Fe(He) and Fe(H), respectively.

In Fig. 2 we show the flux ratios of the Fe lines in the 6.9–7.0 keV to the 6.4–6.75 keV energy ranges as function of the temperature T_0 for a homogeneous isothermal iron plasma (dashed line). This ratio is strongly temperature dependent and only the low-temperature part is shown in Fig. 2. For the 'standard jet' with T_0 as base temperature the ratio varies much less (full line), due to the temperature structure and the contributions of lower ionized material in the cooling jet flow. The error bar with the two data points at $T_0 = 40$ keV indicates the variation of the flux ratios when the initial density of the jet is changed ($n_0 = 10^{13}$ cm^{-3} for the upper point, $n_0 = 10^{14}$ cm^{-3} for the lower data point) indicating the strong role played by density effects in the differentially cooling jet. These two points thus define the minimal inherent uncertainties for a temperature determination via the Fe-line ratios; at this temperature the error is of the order of $\sim 18\%$.

The other symbols refer to models for which the CIE assumption or the standard conical outflow model were abandoned; they will be discussed in the following chapters.

The directly measurable quantities are the strengths of the emission lines, integrated over the visible parts of the jets. In Fig. 3 we plot the emission from different prominent lines, integrated from infinity inwards to the actual position along the jet. This means, the value at length l_j gives the observed line emission from the jet, if only the outer parts $l \geq l_j$ are visible, i.e., if the jet is obscured from its base up to a length l_j.

If the total jet is visible the above mentioned Fe-line ratio will be measured, any partial obscuration of the inner jet will yield a line ratio reflecting the jet temperature at this position. Fig. 3 further demonstrates that most of the Si emission originates in the outer parts of the jet with a very steep gradient along the jet.

2.2. Non-equilibrium ionization

The plasma in the conically out-flowing jet is usually assumed to be in ionizational equilibrium at the local temperature T(l). This approximation is justified for jets with high gas densities. The ionizational equilibration time scale for highly ionized iron is of the order of $n_e\, t \geq 10^{12}$ s cm^{-3} (Brinkmann 1992). With a typical flow time scale of about 100 s this condition can be fulfilled easily for higher density jet models. However, at lower densities and in the outer parts of the jet where the cooling time scales are short deviations from equilibrium conditions can be expected.

We calculated the ionization structure of a conically outflowing jet ($n_0 = 5 \times 10^{13}$ cm^{-3}) by following numerically the ionizational evolution of the plasma (for details of the method see Brinkmann et al. 1989b). It turns out that for the highly ionized species of the heavier elements with prominent emission

lines in the X-ray range, the deviations of the ionization structure from equilibrium conditions remain minute and observationally negligible compared to other model uncertainties.

Lowering the initial density of the jet has two consequences. First, the collision time scales between ions and electrons get longer and the jet itself cools more slowly, resulting in a geometrically longer jet with longer flow time scales. However, even at an initial density of $n_0 = 5 \times 10^{12}$ cm^{-3} the highly ionized iron species are still close to ionizational equilibrium conditions. Only the lower ionization stages of Fe and the lighter elements with lower ionization energies show deviations from CIE in the outer rapidly cooling parts of the jets at temperatures $T \lesssim 10^6$ K. However, these outer jet regions might not be accessible for plasma diagnostics as the ASCA observations indicate that there is interaction of the jet material with extended gas in the system (Kotani et al. 1996).

2.3. Photoionization

The role of photoionization of the gas in the outer X-ray jet by the intense radiation field of the innermost jet is, again, strongly density dependent. For 'standard' jets the optical depth along the jet is of the order of $\tau_{\rm ph} \geq 1$ so that marked deviations from CIE conditions can be expected. The fact that the jet emerges from the disk at a high temperature indicates the existence of a strong radiation field at the base of the jet. If inside the disc's acceleration region black body conditions are reached the luminosity radiated into the cone of the jet will be sufficient to provide the kinetic energy flux of the jet. However, if the Thomson optical depth along the jet is greater than one, which is the case for the above 'standard jet', the scattered radiation will contribute significantly to the jet's observable emission. As there are no observational indications for this component either the density of the jet is lower, reducing the optical depth, or the black body flux emerging from the acceleration region in the disc into the jet is highly diluted. In any case, the emission line ratios can change considerably, making the emission line temperature diagnostics inaccurate.

We have modeled the influence of photoionization by assuming that the emission at the base of the jet can be approximated by a black body spectrum, however, with reduced total flux. For simplicity, we have restricted the photoionization calculations to iron only as the Fe lines in the 6–7 keV range are used as indicators for the plasma conditions. We treated the radiation flux along the jet in a simple optically thin scattering approximation, i.e., the ionizing flux at a distance l from the jet origin is given by

$$I(\nu, l) = I_o(\nu) \times exp[-(\sigma + \alpha_\nu) \times l])$$

where σ is the Thompson scattering cross-section and α_ν the frequency dependent photoionization cross sections for iron which were taken from Reilman & Mason (1979). We have treated in our calculations ionization stages higher than Fe XVI only, which are dominant at temperatures $\gtrsim 5 \times 10^6$ K. Lower plasma temperatures occur far out in the jet ($l \gtrsim 8 \times 10^{11}$cm) where the densities and thus the residual optical depths are small. Scatter-

ing and absorption across the jet was neglected and in the conical jet outflow there are no angular variations of the parameters. The non-equilibrium calculations of the ionization structure were supplemented by extra terms for the formation rate of an ion Fe^{+i} by photoionization of the ion Fe$^{+(i-1)}$ and a destruction rate of the Fe^{+i} ions being photoionized into Fe$^{+(i+1)}$.

For the 'standard' jet parameters and an ionizing black body flux which does not dominate the final jet emission the changes in the iron line ratios are relatively small (see the triangle in Fig. 2) and probably not distinguishable from other systematic differences. The deviations from the collisionally ionized jet get larger for lower jet densities, but not drastically. In any case the scattered component of the photon flux from inside the disk leads to changes of the spectral slope of the jet emission, predominantly at higher X-ray energies due to the high temperatures at the jet's base which might cause a considerable overestimate of the temperature of the out-flowing plasma. This energy range will be best covered with high sensitivity and spectral resolution by the PN camera on board XMM-Newton.

3. Two dimensional outflow

3.1. Effects of lateral expansion

Although the local velocity of sound of the hot gas in the jets is far below the relativistic speed of the outflow, lateral deviations of the jet properties from a simple 'box profile' must be present, even if the jet initially starts with box-like density and temperature profiles. We determined this structure by following the temporal evolution of a two dimensional, axisymmetric, initially conically, hydro-dynamical out-flowing jet until it reaches quasi-stationarity. We used the explicit 3-D Eulerian PPM hydro-code **Prometheus** (Fryxell et al. 1989) and employed a spherical coordinate system with 151×62 zones on a radially and angular non-uniformly spaced grid covering a length of 10^{13} cm and an angular region of 25 degrees in half-angle.

In Fig. 4 we show the density and temperature profile across a jet at a distance of 5.1×10^{11} cm from its origin. Clearly visible is the widening of the density profile (full line) compared to the original box-like distribution (dashed line) and a similar variation of the temperature distribution (diamonds, normalized to the temperature on axis, $T \sim 6.5 \times 10^6$ K). Near the axis the values for the conical and the hydrodynamic jet are still the same. At larger angles the temperature rises to very high values due to the presence of a strong standing shock which forms in the interaction of the expanding jet with its surrounding medium. This spread gets progressively larger with radial distance from the origin of the jet. However, the only directly measurable quantity is the thermal radiation from this out-flowing matter and as the emission is basically proportional to the gas density squared, the outer regions of the jet do not contribute substantially to the observable X-ray flux.

In Fig. 5 we compare the X-ray emission as observed from Earth from the conical jet (dotted histogram) with the emission from the hydro-dynamical outflow (full line). The continuum shapes are nearly identical, however, the hydro-dynamical out-
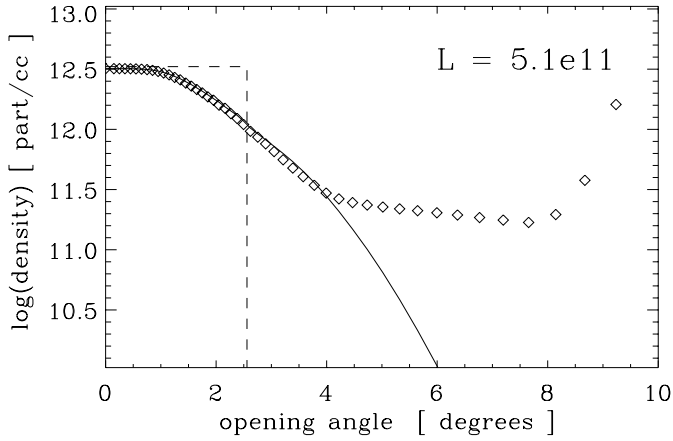
Fig. 4. Logarithmic density and temperature profiles across a jet at a distance of 5.1×10^{11} cm from its base. The dashed line represents the conical 'box profile', both for the density and the suitably normalized temperature. The full line represents the density distribution of the laterally expanding hydrodynamic outflow; the temperature (diamonds) is normalized to the axial value.
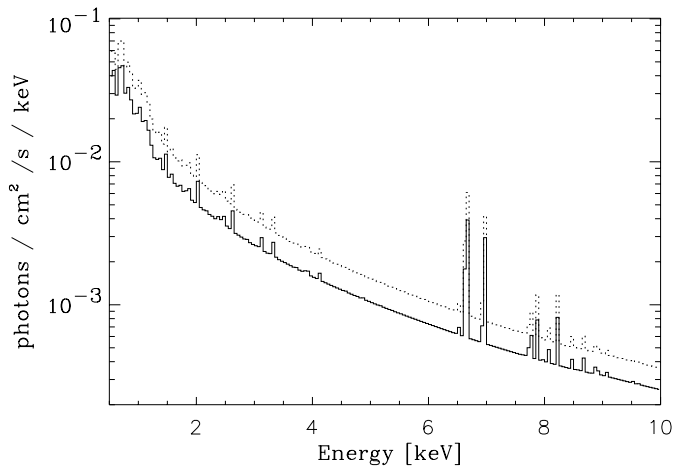

Fig. 5. Photon spectra of a conical jet (dotted histogram) and of a hydrodynamical outflowing jet (full lines).

flow produces about 30% less thermal radiation. This is due to the on average lower density of the laterally spreading jet and the cooling during the expansion. Thus, a simple determination of the jet's density based on the conical outflow model would underestimate the gas density in this case by about 15%.

The differences in the strength of the emission lines seen in Fig. 5 will be hard to disentangle from variations in the temperature profile, ionization structure, or abundances – even with future instruments. Therefore, the determination of the parameters of individual lines alone does not provide strong constraints on the physical parameters of the jets. However, there are strong variations of the emission properties along the jet which can provide an exciting diagnostic tool for X-ray observations with high spectral resolution and excellent statistics.

In Fig. 6 we plot the emissivity (in photons/s/unit length) along the jet for Hydrogen-like and Helium-like iron lines (and, for comparison, of the sum of the He-like Si XIII line at ~ 1.86
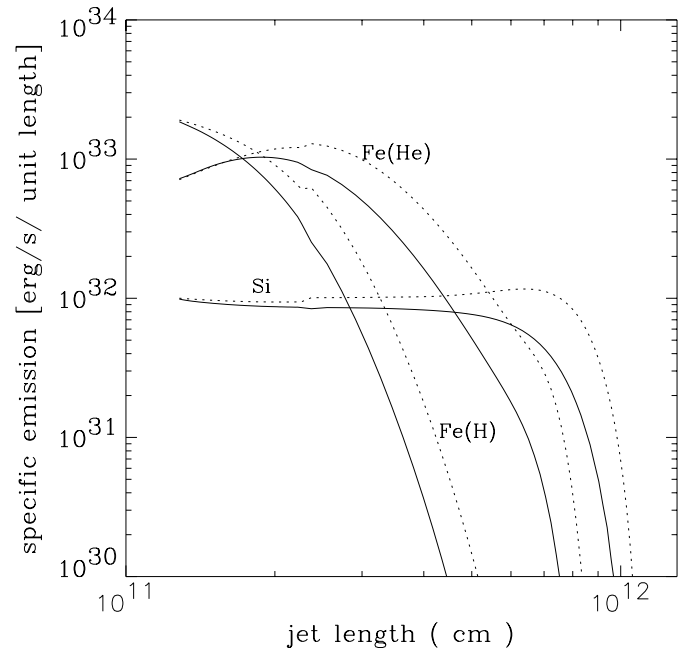
Fig. 6. Line emissivity along the jet for H- and He-like iron ions and silicon). Dotted lines denote the emission from a conical outflow, the hydrodynamical out-flowing jet is given as full lines.

keV and the H-like Si XIV line at ~ 2.01 keV) for the conical jet model (dashed line) and the hydrodynamical outflow (full line). Clearly visible are the strong differences in the emissivities, especially in the outer parts of the X-ray jets. The figure further indicates that any temperature determination from iron line ratios alone might be very problematic as these ratios depend on the geometry of the outflow.
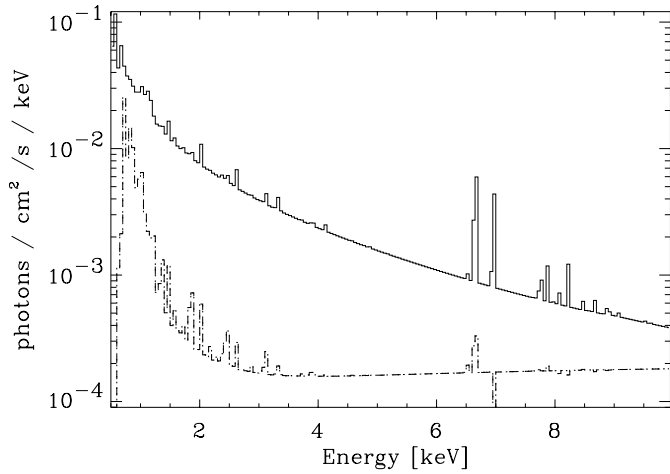
3.2. Non-uniform initial density profile

In the above models the initial density and temperature distribution at the base of the jet was assumed to be constant, i.e. the jet has a flat-top (box-like) density and temperature profile. This choice of boundary conditions ensures that in the conical outflow model the plasma parameters are constant over the jet width and vary only along the length of the jet. Any non-uniform distribution at the jet's base would clearly lead to a differential evolution of the plasma parameters and thus to internal matter flows. However, there is no physical reason for the choice of the box-like density and temperature distribution; in nature it will be determined by the physical conditions resulting in the initial acceleration and focusing of the jets.

To get some estimates about the observational consequences of a non-uniform density distribution we performed two dimensional hydrodynamical simulations of a jet with an initial isothermal Gaussian density distribution, i.e.:
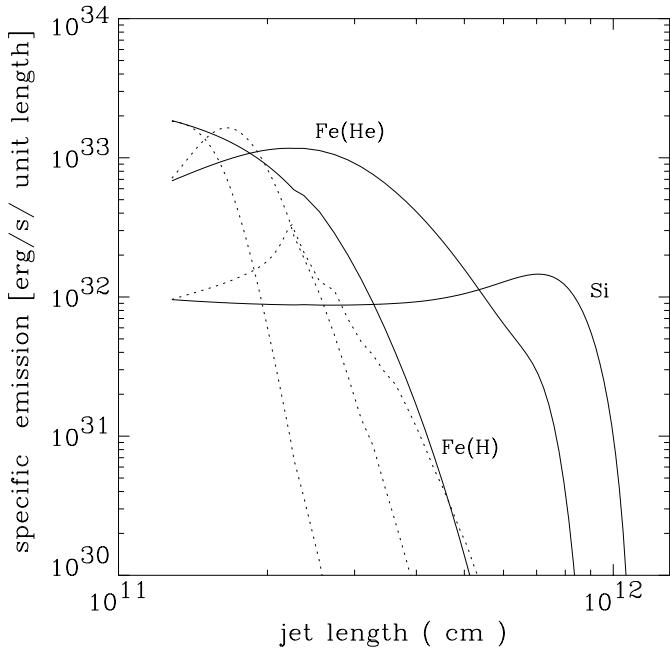
$$n_0 = A_0 \times e^{-\left(\frac{\Theta}{\Theta_o}\right)^2}$$
$$k\,T_0 = 20\,keV$$

The half-width of the distribution was chosen to be $\Theta_0 = 0.75^o$ so that the jet density at angles $\gtrsim 2.5^o$ approaches the
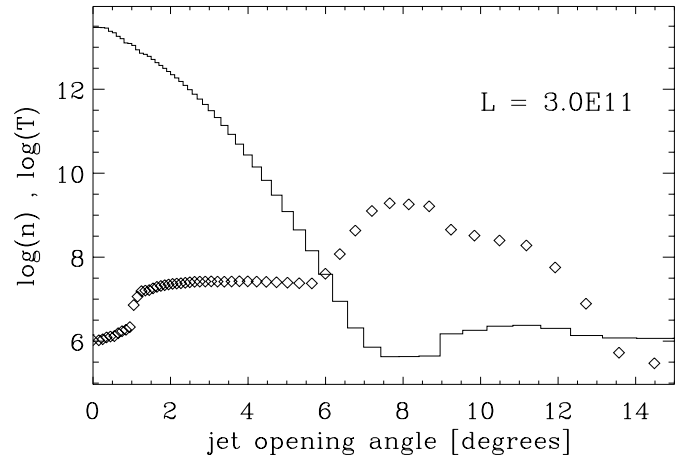
Fig. 7. Photon spectra of a conical jet (full line) and the differences to a hydrodynamical out-flowing jet with an initial Gaussian density profile (dotted histogram).

Fig. 9. Angular profiles of the density (full line) and temperatures (diamonds) across the Gaussian jet at a distance of $\sim 3 \times 10^{11}$cm from its origin

Fig. 8. Line emissivity along the jet for various ions for the conical outflow (full lines) and from a hydrodynamical out-flowing Gaussian jet (dotted lines).

ratio (the '+' in Fig. 2) is nearly undistinguishable from that of the conical jet. Only at lower energies the spectral differences are larger but still too small to be noticed in current X-ray observations.

While the line emission integrated along the whole jet does not provide a useful diagnostic tool the local emission along the jets differs considerably from the conical outflow as shown in Fig. 8. Due to the initial Gaussian density distribution the dense matter on the axis cools much more rapidly than at larger angles leading to a complex temperature and emission structure in the jet. The higher ionized species are found much closer to the base of the jet and the Si-line emission even shows a peaked structure at a distance of $\sim 2.5 \times 10^{11}$cm. A cut through the jet slightly further out, at 3×10^{11}cm is seen in Fig. 9. Plotted are, logarithmically as function of the opening angle the number density (full line) and the temperature structure (diamonds). The jet has widened (the spatially non-uniform expansion velocities reach a few$\times 10^8$ cm/s) and strongly cooled on the axis. In a complex manner, depending on the temperature and density profiles, the maximum of the emissivity moves towards larger off-axis angles in the jet, in a spectrally energy-dependent pattern.

4. Conclusions

The physical parameters of the jets of SS433 are, compared to other astrophysical jets, exceedingly well determined. However, the deduction of the values have depended to a large degree on the assumption of a conically out-flowing jet of matter in equilibrium ionization conditions. We have demonstrated how various second-order deviations from the simplest model change the emission pattern of the radiation and thus lead to systematic errors in the determination of the jets' parameters. The uncertainties are, however, comparable to the inherent uncertainties resulting from the limited statistics and energy resolution of previous X-ray instruments as well as on the inability to discriminate between the different models observationally.

background density. The peak density on axis was determined to be $A_0 = 3.6 \times 10^{14}$ cm^{-3} such that the jet has a similar X-ray luminosity as the standard jet. With these parameters the kinetic energy output amounts to $L_{kin} \sim 5.7 \times 10^{39}$ erg s^{-1}, which is only about one third of that of the standard conical jet.

Fig. 7 shows as full line the photon spectrum of the standard conical jet and as dashed line the difference between this spectrum and that of the jet with an initially Gaussian matter distribution. For positioning the latter histogram onto the logarithmic plot we have added to it a constant value of 2×10^{-4} photons/cm^2/s/keV. As can be seen at higher energies the continuum slopes are practically identical and even the iron line

Current X-ray missions like XMM-Newton and Chandra provide the sensitivity and spectral resolution to disentangle details in the X-ray emission from the SS433 jets which were previously not possible. However, we have shown that even then the exact determination of single specific parameters of the X-ray emission, for example the Fe-line fluxes, are insufficient for an unambiguous determination of the jet's parameters; the full range of observationally accessible data and a detailed modeling is required to map out which kind of jet nature has chosen to realize for SS433.

References

Allen C.W., 1973, Astrophysical Quantities. 3rd ed., Athlone Press, London

Arnaud M., Rothenflug R., 1985, A&AS 60, 425

Arnaud M., Raymond J., 1992, ApJ 398, 394

Brinkmann W., 1992, A&A 254, 460

Brinkmann W., Fink H.H., Massaglia S., Bodo G., Ferrari A., 1988, A&A 196, 313

Brinkmann W., Kawai N., Matsuoka M., 1989a, A&A 218, L13

Brinkmann W., Fink H.H., Smith A., Haberl F., 1989b, A&A 221, 385

Brinkmann W., Kawai N., Matsuoka M., Fink H.H., 1991, A&A 241, 112

Brinkmann W., Aschenbach B., Kawai N., 1996, A&A 312, 306

Fryxell B., Müller E., Arnett D., 1989, MPA preprint, 449

Kotani T., Kawai N., Matsuoka M., Brinkmann W., 1996, PASJ 48, 619

Margon B., 1984, ARA&A 22, 507

Mewe R., Gronenschild E.H.B.M., Van den Oord G.H.J., 1985, A&AS 62, 197

Müller E., Brinkmann W., Plewa T., 2000, A&A submitted

Reilman R.F., Manson S.T., 1979, ApJS 40, 815

Shaham J., 1981, Vistas in Astron. 25, 217

Tanaka K., 1986, PASJ 38, 225

Watson M.G., Stewart G.C., Brinkmann W., King A.R., 1986, MNRAS 222, 261

Yuan W., Kawai N., Brinkmann W., Matsuoka M., 1995, A&A 297, 451